Monolayer Behavior and Langmuir−Blodgett Manipulation of CdS Quantum Dots

Yu-Jen Shen, Yuh-Lang Lee,* and Yu-Min Yang

Department of Chemical Engineering, National Cheng Kung University, Tainan 70101, Taiwan

Received: January 20, 2006; In Final Form: March 16, 2006

Cadmium sulfide (CdS) quantum dots (QDs) were prepared and surface modified by dodecanthiol or mercaptosuccinic acid (MSA) to render a surface with alkyl chains (C_{12}-CdS) or carboxylic acid groups (MSA-CdS), respectively. Due to the hydrophobic property of C_{12}-CdS, the nanoparticles disperse well in chloroform and stay stable at the air/water interface. However, 3-dimensional (3D) aggregative domains and particle-free pores were formed in the monolayer due to poor particle−water interaction. For the MSA-CdS nanoparticles, the surface was hydrophobized through physical adsorption of a cationic surfactant, cetyltrimethylammonium bromide (CTAB). The capped MSA on the CdS plays an important role in enhancing the adsorption of CTAB and improving the stability of the QDs at the air/water interface. Due to the reversible adsorption of CTAB on MSA-CdS, a hydrophilic area can be exposed in the water-contacting region of a nanoparticle when it stays at the air/water interface. Thus, the CTAB-MSA-CdS QD behaves as an amphiphilic compound at the air/water interface and has properties superior to those of C_{12}-CdS QDs in fabrication of layer-by-layer 2D structure of particulate films. The distinct behaviors of the two QDs at the air/water interface and the related effect on the properties of LB films were studied using a number of methods, including pressure−area (π−*A*) isotherm, relaxation and hysteresis experiments, in-situ observation of Brewster angle microscopy (BAM), the postdeposition analysis of atomic force microscopy (AFM), and UV−vis spectroscopy.

Introduction

Semiconductors quantum dots (QDs) have recently attracted extensive interest due to their unique photoelectrochemical properties that arise from the quantum-size effect.[1−3] The photoelectronic and catalytic properties of the QDs can be adjusted by changing the size of nanoparticles[4,5] or by changing the functional groups of molecules capping on the nanoparticles.[6,7] To be utilized in solid devices, the QDs should be immobilized onto solid substrates. Therefore, their application potentials rely largely on the available techniques employed to assemble the nanoparticles.

Various attempts to immobilize the quantum-size particles onto solid substrates have been reported, including the direct synthesis of nanocrystals on solid surface[8−10] or immobilization of preprepared nanoparticles through the use of a self-assembly monolayer[11−15] or by way of the Langmuir−Blodgett (LB) technique.[16−20] Although self-assembly techniques have the advantage of being versatile and fast, LB deposition offers the possibility of fabricating particulate films into a compact, ordered, and controllable structure.

The applications of LB technique to fabricate nanoparticulate films may be approached through three strategies: (1) by postdeposition treatment (heat treatment or exposure to H_2S) of the LB films containing precursors of QDs;[16,21−23] (b) by utilizing the electrostatic interaction between a Langmuir monolayer and the preprepared particles dispersed in the subphases;[24−26] (c) by the direct spreading of surfactant-capped particles at the air/liquid interface.[27−30] The first approach has been extensively used to fabricate quantum dots of II−VI semiconductors through the interaction of a fatty acid monolayer with the metal ions in subphase. The metal ions containing LB film were then exposed to dihydrogen chalcogenides (H_2X, X = O, S, Se, Te) to form the semiconductor chalcogenide nanoclusters (e.g. CdS). The possibility of constructing organic/inorganic LB films with controlled molecular level thickness offers the possibility of fabricating a wide range of nanostructures. Nanoclusters with shapes of spheres,[31−33] thin sheets,[34] disks,[16,35] and ellipsoids[36] have been reported. The numerous structures described in the literature imply the high complexity of the formation kinetic in the LB matrix and the difficulty in controlling the shape and size of the nanoclusters through this approach. As an alternative, the other two strategies provide effective methods to control both the structure and size of QDs, although these strategies have been studied less extensively. For the third method, the direct spreading and compression of the QDs at the air/liquid interface could result in 2-dimensional (2D) monolayer films. This assembly technique not only has the advantage of easy manipulation but also the possibility in controlling the interparticle distance and establishing a closely and regularly packed structure.

For a particulate monolayer at the air/liquid interface, the surface wettability of particles is a critical parameter in determining the monolayer behavior and the 2D arrangement of the particulate film. Particles with highly hydrophilic properties are difficult to keep stable on the surface of an aqueous subphase, and therefore, surface hydrophobization is required to obtain a stable monolayer of particles. The surface hydrophobization is always accomplished by capping alkyl chains on the particle surfaces, either via chemical graft[37−39] or by physical adsorption.[40,41] The monolayer behavior and the quality of particulate film have been reported to be strongly dependent on the degree of surface hydrophobicity, as well as the capping method used. Those studies were performed mainly by using silica particles (with diameters of hundreds nanometer) and novel metals (with quantum size diameters). Only a few studies

* Corresponding author. Tel: 886-6-2757575 ext 62693. Fax: 886-6-2344496. E-mail: yllee@mail.ncku.edu.tw.

10.1021/jp060416k CCC: $33.50
Published on Web 04/22/2006

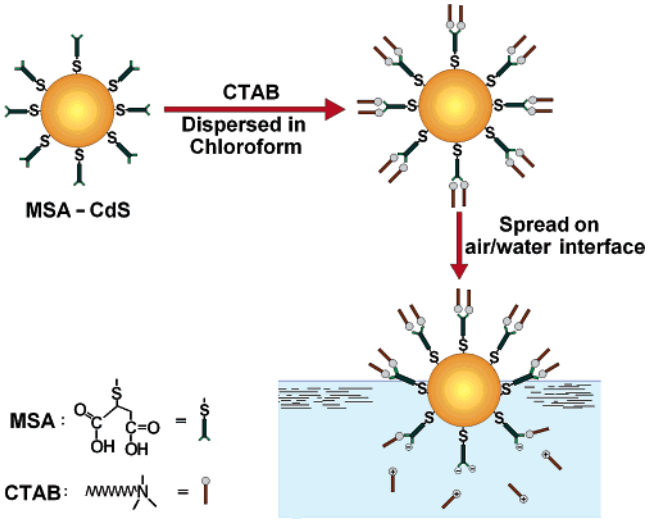

Figure 1. Schematic illustration showing the adsorption of CTAB on a MSA-capped CdS QD and its behavior when the QD was positioned at the air/water interface.

regarding the particulate monolayer of semiconductor QDs have been done.[24,25,27−29]

For particles chemically modified by alkyl chains, the modifiers distribute uniformly on the particles' surface. Therefore, the particles do not develop the amphiphilic characteristics of surfactant molecules. When such particles are spread at the air/water interface, the weak particle−water interaction results in the formation of void defects or 3D aggregates in the monoalyer.[42−44] Various approaches have been adopted to enhance the spreading of particles at the air/water interface, of which the physical modification of particle surface may be the most efficient method.[43−46] The effects of chemical and physical modifications of the particle surface on the monolayer behavior of silica particles and the related structure of the particulate films were studied in our previous research.[43] In this work, this strategy is utilized to the organization of CdS QDs. Mercaptosuccinic acid (MSA) is first capped on the CdS surface to render a surface with carboxylic acid groups. Such modification was found to enhance the adsorption of cationic surfactant on the CdS surface, improving the stability and film quality of the CdS monolayer. This strategy is schematically illustrated in Figure 1. The results of this approach are also compared with those obtained from dodecanethiol-capped CdS.

Experimental Section

Materials. Cetyltrimethylammonium bromide (CTAB, >96%, Fluka), cadmium nitrate ($Cd(NO_3)_2$, >99%, Fluka), sodium sulfide (Na_2S, >98%, Aldrich), mercaptosuccinic acid ($HOOCCH_2CH(SH)COOH$, MSA, >97%, Aldrich), *n*-hexane (>99%, Riedel-deHaen), ethanol (>99%, Merck), butanol (>98%, Riedel-deHaen), dodecanethiol (>98%, Acros), and chloroform (>99.8%, Mallinckrodt chemicals) were used as received. Doubly distilled water (resistivity ≥18.2 MΩ cm) purified with Milli-Q apparatus supplied by Millipore was used in all the experiments of this study.

Synthesis of CdS Particles. CdS QDs were prepared using the water-in-oil reverse micelle process similar to that reported by Agostiano et al.[47] A quaternary water-in-oil microemulsion, CTAB/*n*-butanol/*n*-hexane/water, containing cadmium or sulfide was prepared first by controlling the molar ratio of water to CTAB (W_0), butanol to CTAB (P_0), and the surfactant concentration of CTAB. The values of W_0 and P_0 were both controlled at 15, and a CTAB concentration of 0.1 M was used in this work. Colloidal CdS QDs were prepared by rapidly mixing equal volumes of two micellar solutions containing respectively 0.5 M $Cd(NO_3)_2$ and 0.5 M Na_2S, introduced in the microemulsions as aqueous solutions. CdS QDs formed immediately after mixing the micellar solutions, and the following surface modification procedure was carried out by adding dedecanethiol or MSA directly into the micellar solution. The surface reaction occurred during 24 h of continuous stirring. After the synthesis and modification steps, the microemulsion was evaporated at 50 °C under vacuum to remove hexane. The residue (containing CdS, butanol, water, surfactants) was then dissolved in ethanol. This ethanol solution was turbid, and its centrifugation allowed separation of a pale yellow powder as a pellet. The collected crystallites were washed five times with an ethanol/water mixture (8/2 by volume) to remove, as completely as possible, the dissolve salts and water-soluble compounds. The powder was then dried under an N_2 stream and stored in the dark. The dodecanethiol-capped CdS was redispersed in chloroform, and the MSA-capped CdS was redispersed in chloroform containing 2000 ppm of CTAB.

Monolayer Preparation. The modified CdS QDs were redispersed in chloroform to prepare a stock solution with a concentration of ca. 2−4 mg/mL. The exact content of CdS QDs in the solution was determined by TGA (Thermo Gravimetric Analyzer).

The monolayer experiments were performed in a computer-controlled film-balance apparatus (KSV minitrough) constructed by KSV Instruments Ltd., Finland. The Teflon trough has a working area of 32 × 7.5cm^2 and was placed on a vibration isolation table and enclosed in an environmental chamber. The temperature of the subphase was controlled at 25 °C by an external circulator, and the film pressure was measured by using the Wilhelmy plate arrangement attached to a microbalance. A stock solution of CdS QDs (ca. 100 μL) was spread on the subphase using a microsyringe. After allowance of 20 min for solvent evaporation, the monolayer at the air/water interface was compressed at a rate of 5 mm/min. A surface pressure−area ($\pi-A$) isotherm was obtained by continuous compression of the monolayer by two moving barriers.

Optical glasses were used as the substrates for deposition of the particulate monolayer. The glass plate was carefully cleaned and had a measured contact angle of 0° with water. A hydrophobic glass slide was prepared by dipping the cleaned glass plates in chloroform solution containing 1 wt % dedecyltrichlorosilane. The advancing contact angle of water on the hydrophobic glass plate was about 108°. In this work, LB deposition (vertical deposition method) cannot be satisfactorily used to transfer the C_{12}-CdS monolayer. Therefore, to examine the morphology of a single layer of particulate film, all the monolayers were transferred by reducing the liquid level of the subphase as described in a previous work.[43] Using this technique, the arrangement of QDs at the air/water interface appears to be better preserved on the solid substrate. A glass plate was first positioned beneath the monolayer with an incline angle of 10° to the horizontal plane. After compression of the monolayer to a selected surface pressure (15 mN/m), the subphase liquid was withdrawn smoothly. The level of the monolayer surface decreases gradually, and thus the monolayer touches the substrate and deposits on it gradually. To prepare multilayer particulate film, the LB deposition was employed at a transfer rate of 3 mm/min.

Instrumentation and Characterization. The particulate monolayer at the air/water interface was observed in-situ using a Brewster angle microscope (BAM) designed by Nanofilm

Technology (NFT), Göttingen, Germany (model BAM2 plus). For this experiment, a larger trough constructed by Nima Technology Ltd., England (model 601 BAM), was used. The trough has a working area of 70 × 7 cm^2, which is large enough to mount the BAM directly onto it. The images were captured using a CCD camera and were recorded by means of a video recorder. The lateral resolution of the BAM was about 2 μm. The morphology of the particulate film was examined using an atomic force microscopy (AFM) (Digital Instruments Inc., NanoScope IIIa) via the tapping mode. A silicon tip on a cantilever with a length of 100 μm (noncontact silicon cantilever, Silicon-MDT Ltd.) was used.

Fourier transform infrared (FT-IR) spectra of the QDs were measured with a Perkin-Elmer Spectrum GX, using a KBr pellet. UV−visible absorption spectra were analyzed with a UV−visible spectrometer constructed by GBC Scientific Equipment, Australia (model GBC Cintra 10e). TEM observation was performed using a high-resolution transmission electron microscope (Hitachi H-7500). The TEM specimen was prepared by dropping the stock solution of CdS (dispersed in chloroform) on a carbon-coated copper grid, allowing the evaporation of the chloroform.

Results and Discussion

After surface modification, the dodecanethiol-capped CdS (C_{12}-CdS) QDs were dried and redispersed in chloroform. Satisfactory dispersion was confirmed by the transparency of its yellow solution and by the observation of TEM. A similar condition can also be obtained by dispersing the MSA-capped CdS (MSA-CdS) QDs into chloroform containing 2000 ppm of CTAB. Without the capping of MSA, or in the absence of CTAB in chloroform, a transparent solution cannot be obtained. Although CdS QD was reported to have negative ζ potential (ca. −20 mV),[24] the adsorption of CTAB from chloroform to a bare CdS surface was not able to perform well in this work. This result is attributable to the low potential of the CdS surface because the CTAB adsorption does perform well on silica nanoparticles which have a higher ζ potential (ca. −57 mV).[43] Therefore, the MSA capped on the CdS surface plays an important role in adsorbing the CTAB molecules, a conclusion also confirmed by the higher ζ potential of MSA-CdS (ca. −55 mV). Figure 2 shows the size distributions of the CdS QDs determined by TEM images. The TEM micrograph of C_{12}-CdS is also shown as a representative. The mean diameter of the QDs is 4.9 nm for bare CdS, 5.8 for MSA-CdS, and 6.1 nm for C_{12}-CdS. The size dispersion of CdS QDs increases slightly after the capping process, probably due to the growth of QDs in the long capping process. However, since the sizes of C_{12}-CdS and MSA-CdS are very close, the size effect is negligible in comparing the monolayer behaviors of the two QDs discussed below.

The UV−vis adsorption spectra of the CdS QDs dispersed in solution were normalized to their respective absorbance at 350 nm and are shown in Figure 3. In general, the CdS QDs have nearly identical spectral features both before and after capping. The adsorption edge, obtained from the intersection of the sharply decreasing region of the spectrum with the baseline, is ca. 472 nm for the bare CdS, 482 nm for CTAB-MSA-CdS, and 486 nm for C_{12}-CdS, corresponding respectively to average diameters of 4.4, 4.8, and 5.1 nm, as estimated by Henglein's empirical curve.[48] The mean particle size increases slightly after surfactant capping, consistent with the result determined by TEM. The slight deviation of particle sizes estimated by TEM images and the UV−vis spectrum may be caused by analysis error of the two instruments or from a discrepancy in Henglein's theory.

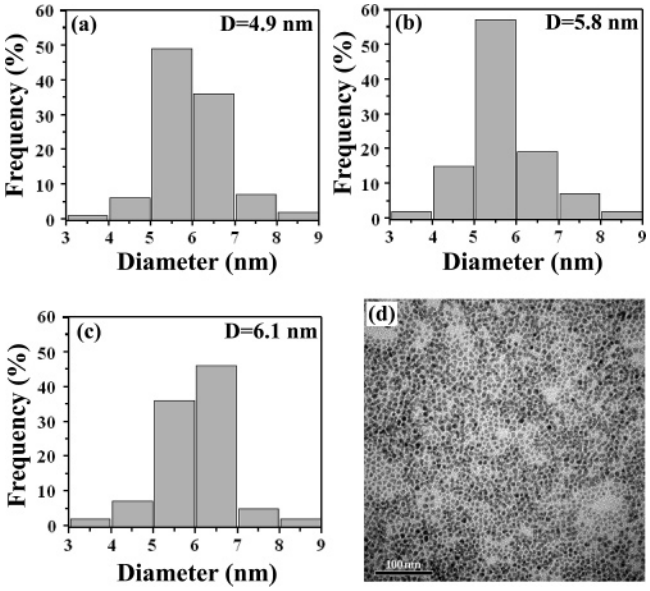

Figure 2. Size distribution charts of bare CdS (a), MSA-CdS (b), and C_{12}-CdS (c) determined from the TEM images. The TEM image of C_{12}-CdS QDs was shown as a representative (d).

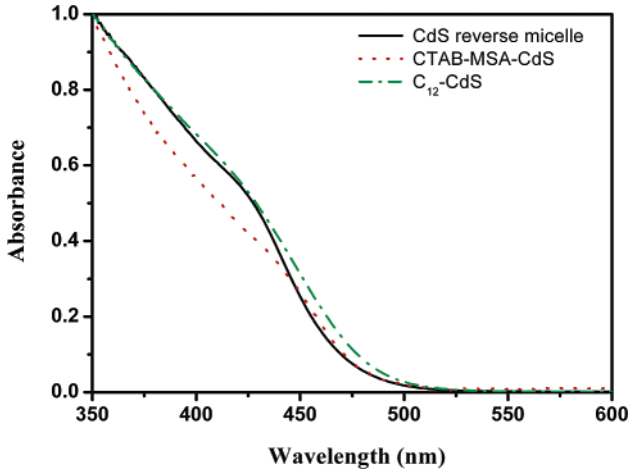

Figure 3. UV−vis spectra of CdS QDs with and without the capping of surfactant. The QDs were dispersed in chloroform (capped) or hexane (uncapped).

A comparison of the FT-IR spectra among pure MSA, bare CdS, C_{12}-CdS, and MSA-CdS is shown in Figure 4. For the spectrum of bare CdS, the weak peaks which occur in the region of 1000−1750 cm^{-1} are ascribable to the contaminants after the purifying process. For C_{12}-CdS, the appearance of peaks at 2954 cm^{-1} ($\nu_{as}(CH_3)$), 2920 cm^{-1} ($\nu_{as}(CH_2)$), and 2850 cm^{-1} ($\nu_s(CH_2)$) indicates the presence of alkyl chains and the formation of dodecanthiolate was further confirmed by the stretching vibration of C−S linkage in the 700−600 cm^{-1} region. The spectrum of pure MSA in this work is similar to the result reported in the literature.[49] When MSA molecules adsorb on CdS QDs, the peaks of carboxylate vibration appear at 1562 cm^{-1} (in the range 1500−1650 cm^{-1}, asymmetric) and 1389 cm^{-1} (in the range 1350−1450 cm^{-1}, symmetric). This result indicates not only that there is attachment of MSA to the CdS but also that the carboxylic hydrogen was dissociated and the MSA is present in the form of a carboxyl anion.[49] However, the weak peak at 1705 cm^{-1} (carbonyl strecting vibration) suggests that few MSA molecules exist in the form of dimmers.

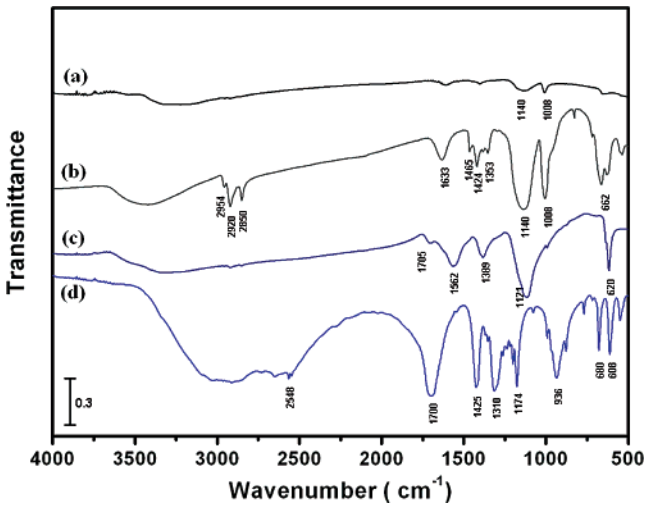

Figure 4. FT-IR spectra of bare CdS (a), C_{12}-CdS (b), MSA-CdS (c), and pure MSA (d).

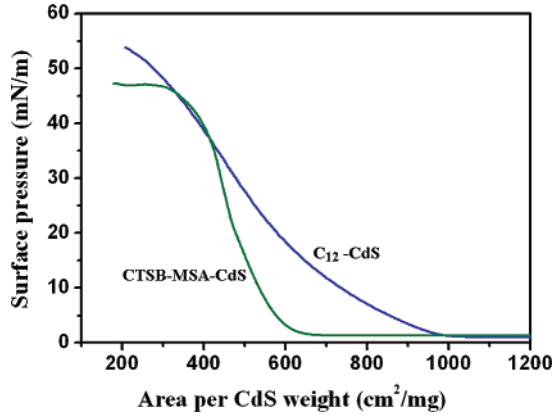

Figure 5. Pressure−area ($\pi-A$) isotherms of C_{12}-CdS and CTAB-MSA-CdS QDs monolayers.

In addition, the disappearance of the peak at 2548 cm^{-1} (S−H stretching) in the spectrum of MSA-CdS gives strong evidence that MSA is anchored on the CdS QDs.

Isotherm Characteristics of CdS Particulate Monolayers. Figure 5 shows the pressure−area ($\pi-A$) isotherms of the CdS QDs at the air/water interface. For the C_{12}-CdS QDs, the isotherm has a lift-off area of ca. 990 cm^2/mg and exhibits a high compressible characteristic as verified by the slow increase of surface pressure as the area is decreased. No apparent phase transition or collapse point was observed in the isotherm. For the QDs modified by physical adsorption of CTAB (CTAB-MSA-CdS), the isotherm has a smaller lift-off area (ca. 630 cm^2/mg) and exhibits a less compressible property when compared with that of the C_{12}-CdS. It should be noted that no significant elevation of surface pressure can be detected under compression when only CTAB or MSA-CdS was spread on the subphase. Therefore, the elevation of surface pressure can be attributed to the interaction of CTAB and MSA-CdS. The collapse point of the monolayer occurs at a surface pressure of ca. 45 mN/m. The limiting areas estimated by extrapolating the constant-slope region of the isotherms to zero surface pressure are about 722 cm^2/mg (39.2 nm^2/particle) for C_{12}-CdS and 537 cm^2/mg (29.2 nm^2/particle) for CTAB-MSA-CdS. The theoretical area calculated for nanoparticles of 6 nm in diameter configured in a hexagonal closely packed arrangement is 31.2 nm^2/particle. According to the AFM results that will be shown later, the higher value of C_{12}-CdS is caused by the formation of particle-free pores due to the poor spreading of C_{12}-CdS on the subphase. But for the CTAB-MSA-CdS, the smaller area compared to the theoretical value is attributable to the loss of nanoparticles into subphase due to the poor stability of this monolayer, a situation which will be discussed later. Furthermore, the size distribution of the QDs may also cause deviation between the estimated and theoretical areas.

The isotherms obtained here are consistent with a previous result which was performed with silica particles of 500 nm in diameter.[43] The compressible characteristic of chemically modified particles has been ascribed to the lack of lateral mobility of particles due to poor a particle−water interaction. However, the reversible adsorption of CTAB on MSA-CdS can yield a hydrophilic region on the QDs when they are positioned on the aqueous phases (as shown in Figure 1). The higher particle−water interaction results in a higher spreading ability of the particles, which also causes the isotherm to be less compressible.

The surface morphology of single layer particulate films transferred at $\pi = 15$ mN/m onto mica was analyzed by AFM and is shown in Figure 6. For the chemically modified CdS (C_{12}-CdS) shown in Figure 6a, the QDs are presented as separated domains of several hundreds nanometers scale. Apparently, the cohesive interaction between QDs is higher than the spreading force exerted by the subphase; thus, the QDs tend to aggregate rather than spread homogeneously. The aggregative domains were found to form in the spreading stage as confirmed by BAM, and the compression causes a shrinkage of the distance between domains but increases their coverage ratio. However, the QD free regions cannot be eliminated completely by decreasing the surface area, and voids can still be observed on films transferred at pressures exceeding 30 mN/m. From a finer scan of the AFM image (Figure 6b), the particulate domains are found to be organizing by irregular packing of CdS QDs. The depth profile analysis shown below Figure 6b indicates that the heights of the domains are not uniform (ranging from 5 to 15 nm) and go far beyond the value of the QD size (ca. 5−6 nm). This result implies that the C_{12}-CdS QDs are organized as three-dimensional (3D) aggregates rather than as 2D domains.

The morphological characteristic of the particulate film prepared with CTAB-MSA-CdS QDs has results (shown in Figure 6c,d) different from those of the films prepared with C_{12}-CdS. The QDs distribute homogeneously without the formation of aggregative domains and pores. Although few aggregations have been observed, they are believed to be the defects caused from the nonperfect dispersion of the QDs in the spreading solvent. The high-resolution scan and related depth profile (Figure 6d) indicate that the film has a thickness approximately equal to the diameter of QDs, which also implies that CdS QDs are organized as a 2D monolayer. The improvement in the 2D assembly of the QDs was mainly ascribed to the amphiphilic property of the QDs resulting from the physical modification of the particle surface.

According to the morphological characteristics and the $\pi-A$ isotherms of CdS QDs presented here, as well as the results of SiO_2 particles reported in a previous study,[43] a large lift-off area and highly compressible isotherm are supposed to be a result of poor lateral mobility of particles, a condition which yields a network structure of particulate film. Therefore, the compressible isotherm of a particulate monolayer may not have properties similar to the monolayer of amphiphilic molecules. In the present case, the appearance of a highly compressible isotherm of a particulate monolayer may suggest the formation of a heterogeneous structure containing particle free pores, with the "compressibility" coming from the shrinkable pores between particulate domains.

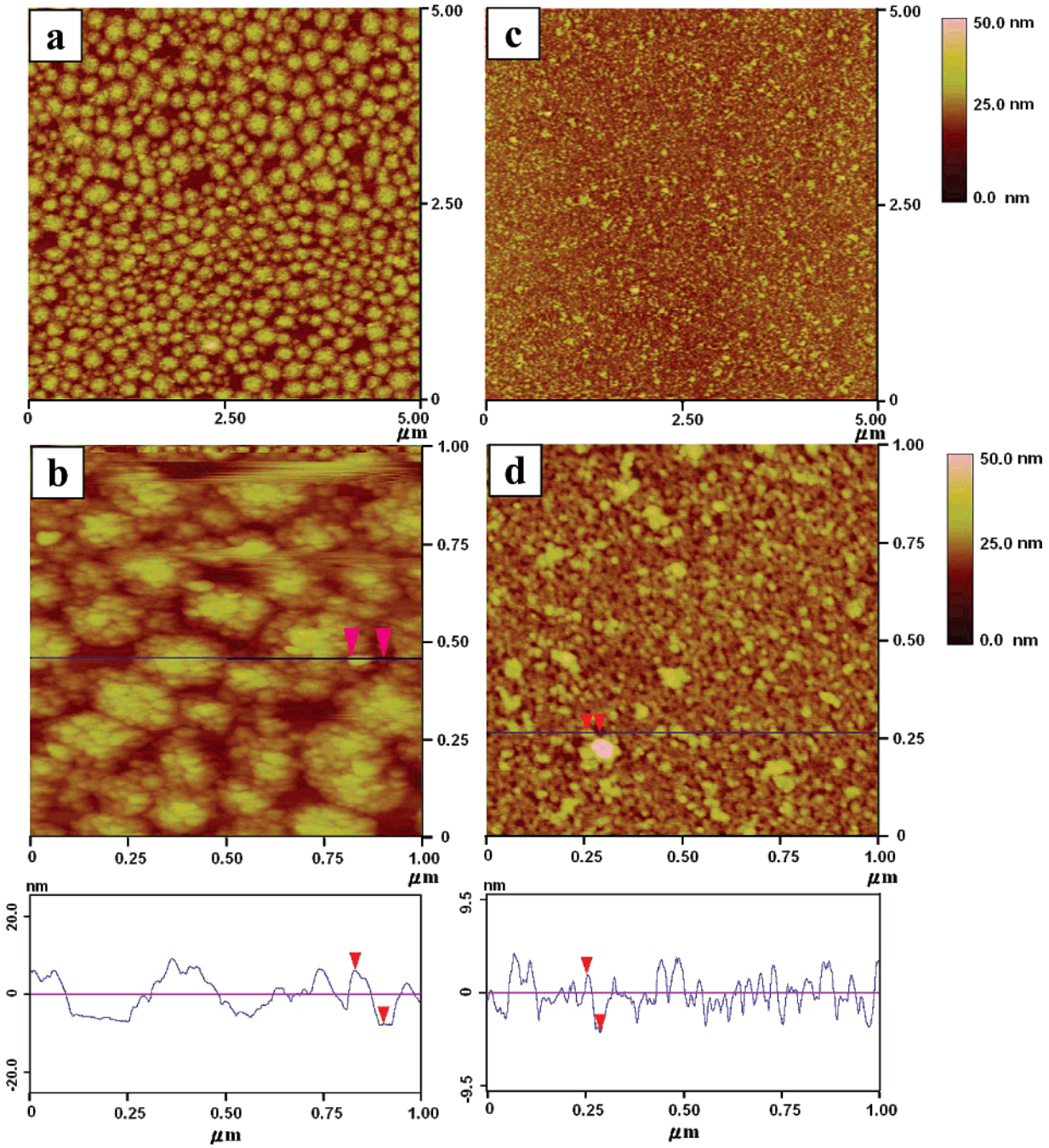

Figure 6. AFM images of one layer C_{12}-CdS (a, b) and CTAB-MSA-CdS (c, d) particulate films transferred from air/water interface to mica at 15 mN/m. To prevent structure distortion induced by the disturbance of interface during LB transfer, the transfer was performed by descending the liquid level of subphase as described elsewhere.[43]

The stability of particulate monolayer was evaluated by the area relaxation of monolayer performed at $\pi = 20$ mN/m. As shown in Figure 7, the area loss of the monolayer after 120 min relaxation is about 4% for C_{12}-CdS, and about 30% for CTAB-MSA-CdS. The chemically grafted CdS QDs are essentially stable at the air/water interface, implying an insignificant growth and coalescence of QDs and their 3D aggregates during the relaxation process. This result also confirms the inference that the 3D aggregates, found in Figure 6a,b, are formed in the spreading stage. On the other hand, the physically modified QDs are relatively unstable, which can be ascribed mainly to the loss of QDs into the water subphase during the relaxation process. Due to the reversible adsorption of surfactants on the physically modified particle, it is possible for a particle to move deep into the water subphase when its surface becomes more hydrophilic due to prominent desorption of surfactant. In general, the results obtained here are consistent with those reported for silica particles,[43] except that the monolayer of CdS is less stable than that of SiO_2 when the particles are physically modified. This difference is probably caused by the different adsorption abilities of CTAB on MSA-CdS and on SiO_2.

The hysteresis curves of the two monolayers shown in Figure 8 demonstrate the compression−expansion behavior of the two QDs at the air/water interface. For the C_{12}-CdS monolayer (Figure 8a), the expansion curve shifts left slightly in respected to the compression one, indicating a small hysteresis due to the low respreading ability of the particles. Besides, the effect of the surface pressure gradient on SiO_2 monolayer[43] was not significant in this study, probably due to the small size of the

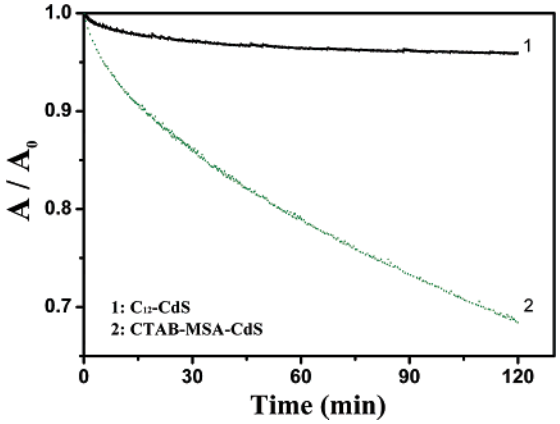

Figure 7. Area relaxation of C_{12}-CdS and CTAB-MSA-CdS particulate monolayers performed at surface pressure of 20 mN/m.

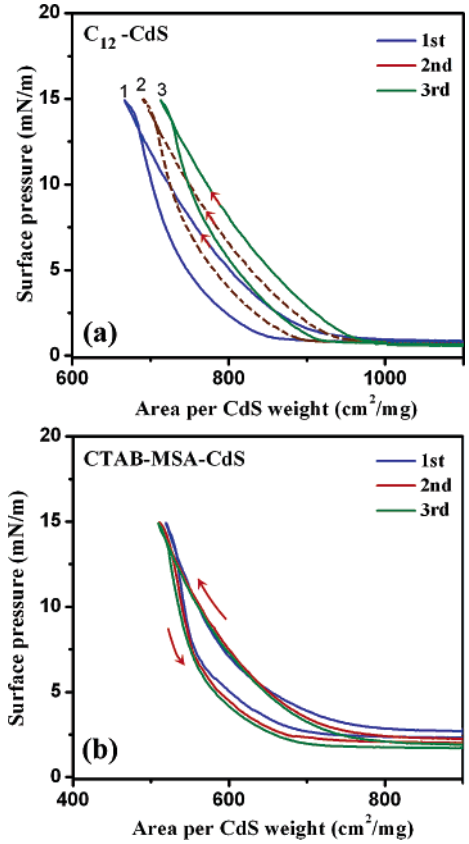

Figure 8. Hysteresis curves show the compression/reexpansion behavior of particulate monolayers of C_{12}-CdS (a) and CTAB-MSA-CdS (b).

CdS QDs. However, it is unusual to find that the hysteresis loop shifts to the right cycle by cycle because it implies a gain of pressure (i.e. the gain of free particles) after each compression−expansion cycle. This phenomenon was studied using an AFM image of particulate film transferred after 3 hysteresis cycles. The results shown in Figure 9 demonstrate that the film morphologies are essentially similar before and after the hysteresis process, but the domain height decreases after the hysteresis experiment. The root-mean-square (rms) roughness measured from Figures 6a and 9a are 4.7 and 2.6 nm, respectively, indicating that the film was flattened due to the push and pull effects of the hysteresis process. This result is consistent with the right shift of the hysteresis loops shown in Figure 8a and is probably a result of the poor spreading of CdS QDs in the initial spreading period.

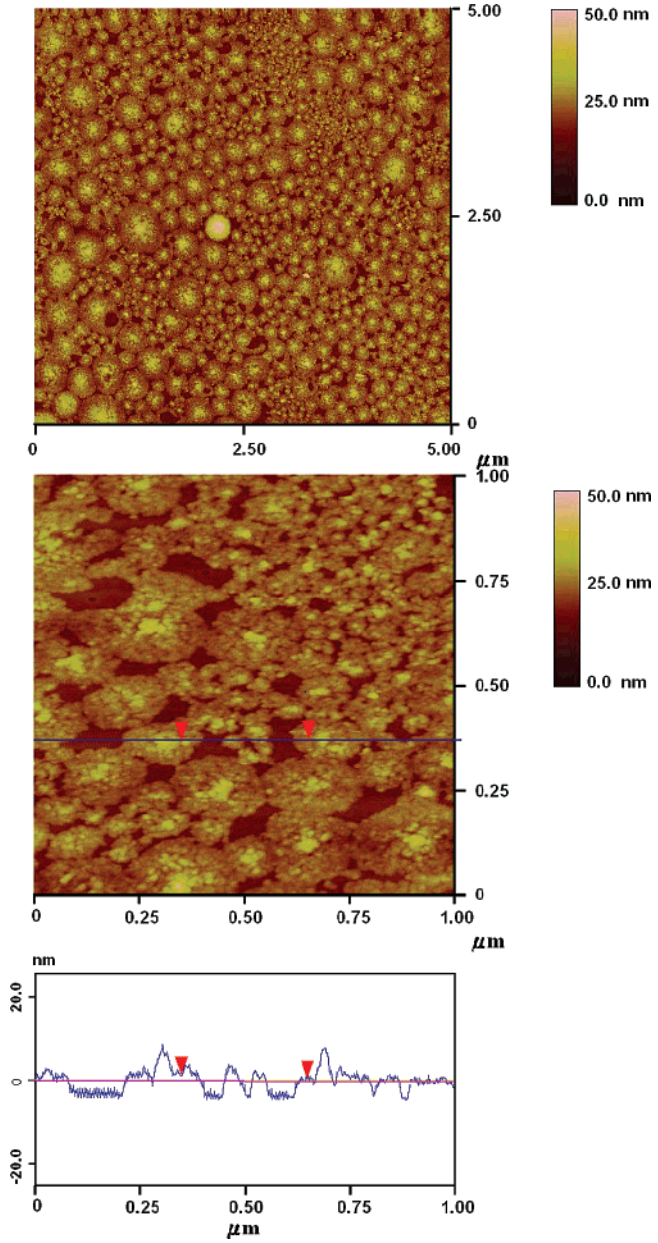

Figure 9. AFM images of one layer C_{12}-CdS transferred after experience three hysteresis cycles at the air/water interface.

The monolayer of CTAB-MSA-CdS exhibits a hysteresis behavior similar to that of the C_{12}-CdS monolayer in each compression−expansion cycle (Figure 8b). A slight hysteresis behavior is also observed in the left shift of the expansion curve. However, the nearly identical loops for the three hysteresis cycles imply that the QDs are able to respread to the initial state in the beginning of the succeeding compression. Therefore, this slight hysteresis can be attributed to a slow expansion rate of the QDs.

BAM Images of CdS Particulate Monolayers. The behaviors of the two CdS QDs on the water surface were also studied using BAM phase images. For the C_{12}-CdS monolayer (Figure 10), two distinct phases were observed in the initial compression stage. They are considered to be part of the coexistence state of liquid and gas phases, similar to that of molecular compounds. The liquid phase exhibits a cloudy morphology consisting of voids distributed among a denser phase. Such phase seems to have a network structure organized by the contact of the particulate domains. However, due to the poor lateral mobility of C_{12}-CdS QDs, the domains are rigid and resist deformation.

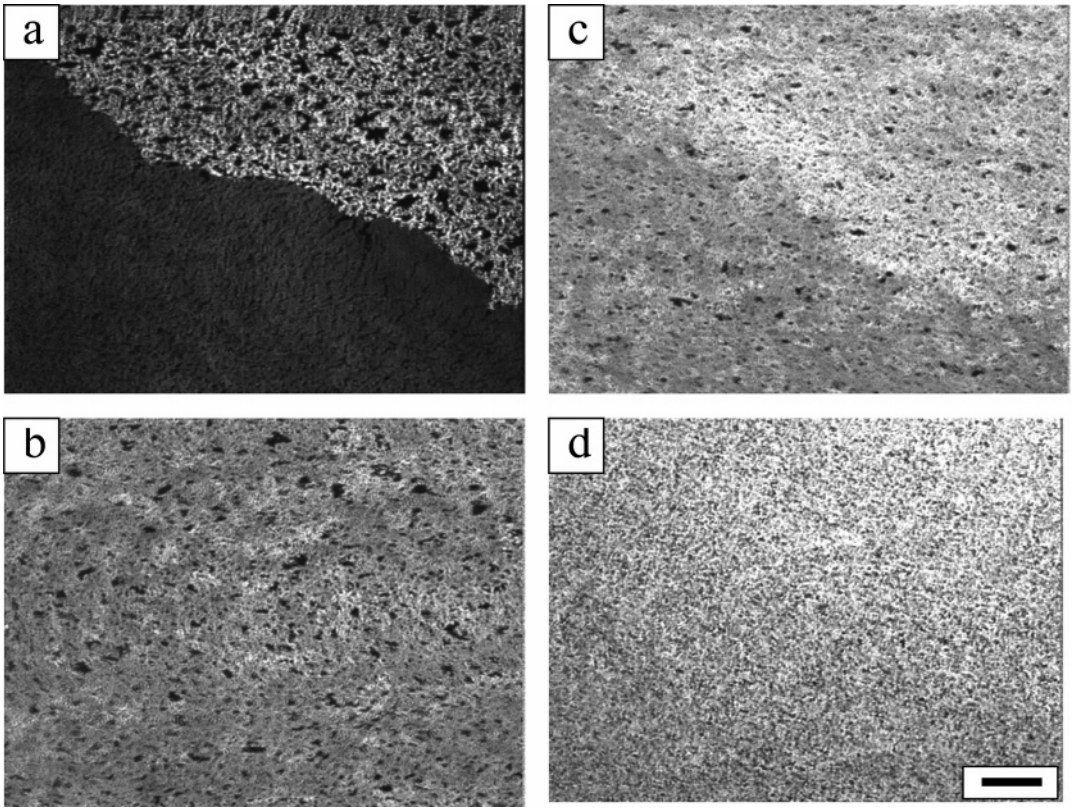

Figure 10. BAM images of C_{12}-CdS particulate monolayer at air/water interface acquired along the compression isotherm. The images correspond to the states of (a) $\pi = 0.9$ mN/m, (b) $\pi = 6.0$ mN/m, (c) $\pi = 22$ mN/m, and (d) $\pi = 35$ mN/m. The length bar corresponds to 50 μm in length.

Therefore, the voids cannot be eliminated by the coalescence of domains. After compression, the gas phase decreases in area and the liquid-phase becomes more condensed. However, the empty pores still present in the condensed phase (as shown in Figure 10b) acquired at a surface pressure of about 6 mN/m. When the pressure increases further, the brightness of the image gradually increases, indicating the increasing density or thickness of the monolayer. A typical image acquired at $\pi = 22$ mN/m (Figure 10c) shows the heterogeneous characteristic of the monolayer. The appearance of high-brightness areas indicates the formation of a highly aggregative structure. When the pressure is elevated above 30 mN/m, the brightness of the image becomes more uniform and the voids shrink. In Figure 10d ($\pi = 35$ mN/m), the voids cannot be clearly observed or identified under the resolution of BAM. However, since the AFM results indicate the presence of voids, the black fine-dots distributing in Figure 10d represent not only the cavities between aggregates but also the voids.

The BAM images for the CTAB-MSA-CdS monolayer (Figure 11) show a morphology different from that of the C_{12}-CdS monolayer. During the initial compression stage, no definable phase was noted, and the state was considered to be the gas phase. At $\pi = 0.3$ mN/m ($A = 900$ cm^2/mg), a phase consisting of dense fine-dots can be observed on the upper region of Figure 11a, indicating the formation of a denser phase (liquid phase). The appearance of a fine-dot structure rather than a uniform phase suggests that the QDs are loosely packed, probably due to the higher particle/water interaction compared with the cohesive interaction between particles. Also note that no apparent phase boundary can be observed between the liquid and gas phases, which is also ascribable to the high spreading ability of the QDs. Upon compression, the gas phase decreases gradually and disappears completely when it reaches a pressure of ca. 5 mN/m. In a fully extended liquid-phase acquired at $\pi = 12.5$ mN/m (Figure 11b), phase heterogeneity can be found as indicated by the nonuniform brightness shown in this figure. Phases with high and low brightness are commonly observed in this monolayer before $\pi = 20$ mN/m and may correspond respectively to the liquid condensed and liquid expanded phases. At about 20 mN/m, a more uniform and condensed phase is imaged as shown in Figure 11c. This phase can be considered as the solid phase, and the uniform structure can be sustained until compression reached approximately 30 mN/m. Above 30 mN/m, an extremely bright region appears due to the collapse of the monolayer (Figure 11d).

Langmuir−Blodgett Deposition and UV−Vis Absorption Spectra of LB Films. LB deposition was employed to prepare multilayer CdS particulate films onto glass plates. When the C_{12}-CdS monolayer is transferred onto hydrophilic glass slides, the transfer ratio is about 0.5 in the first upward stroke but becomes negative in the successive downward stroke. When a hydrophobic glass slide is used, poor transfer ratio is also obtained. This result indicates that multilayer deposition cannot perform well for the C_{12}-CdS monolayer, suggesting the poor adhesion of the particles to the glass substrates. For the CTAB-MSA-CdS monolayer, the transfer ratio onto a hydrophobic glass slide is satisfactory (>0.9) in the first 2 or 3 layers but becomes poor in the following strokes. When the transfer is performed onto a hydrophilic glass slide, the transfer ratio ranges between 0.95 and 1.1 for all the upward strokes, but the downward strokes have a value close to zero. Therefore, a Z-type multilayer LB film was fabricated using the physically modified CdS QDs. It appears that the hydrophilic moiety of the particle can impose a better adhesion of the particle to the hydrophilic substrate. Therefore, the upward-transferred layer can sustain the peeling force exerted by the surface tension in the succeeding downward stroke. The near-zero value of the transfer ratio in the down-stroke indicates that the hydrophobic−hydrophobic interaction

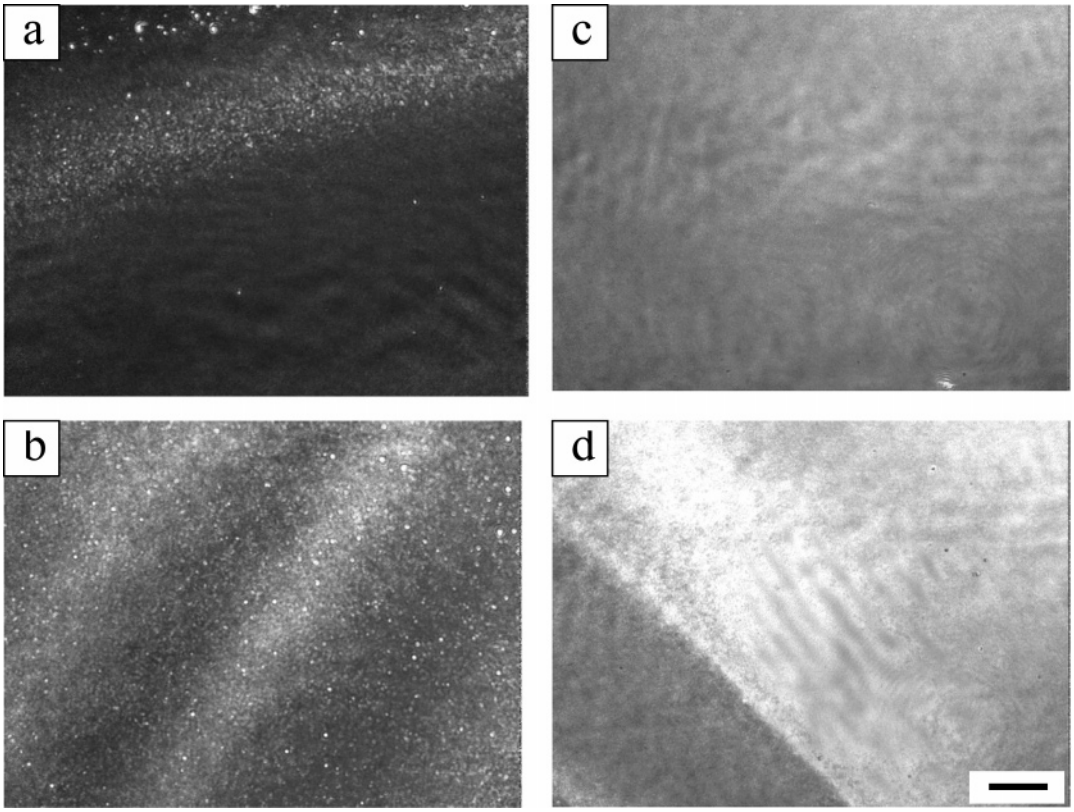

Figure 11. BAM images of CTAB-MSA-CdS particulate monolayer at the air/water interface acquired along the compression isotherm. The images correspond to the states of (a) $\pi = 0.3$ mN/m, (b) $\pi = 12.5$ mN/m, (c) $\pi = 21$ mN/m, and (d) $\pi = 32$ mN/m. The length bar corresponds to 50 μm in length.

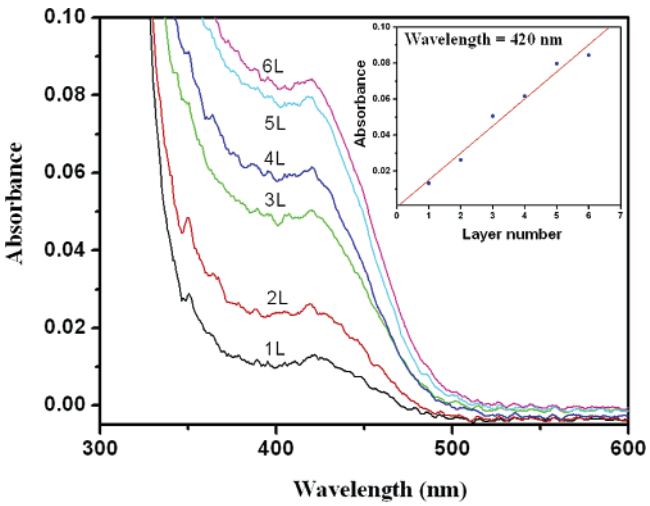

Figure 12. UV−vis spectra of CTAB-MSA-CdS LB films with various deposition layers. The insert plots the absorption intensity at 420 nm vs number of deposition layer.

between particles is not sufficient to pull the particles into the aqueous subphase. Actually, it is quite possible that the adsorbed CTAB will desorb once the QDs are pulled down into the subphase. That is why a poor transfer ratio was obtained in the downward stroke. Additionally, the desorption effect also gives a hydrophilic surface to the particle, allowing the succeeding upward stroke to be performed successfully.

The CTAB-MSA-CdS particulate films were then analyzed via a UV−vis spectrometer. The absorption spectra taken on films of various deposition layers are shown in Figure 12. The absorption edge of these spectra is ca. 489 nm, corresponding to an average diameter of 5.2 nm, according to Henglein's empirical formula.[48] The peak at 420 nm is associated with the first excitonic transition of CdS QDs, and its appearance also implies a narrow particle size distribution of the particulate system. The absorption intensity at 420 nm was found to increase linearly with number of CdS layers (insert of Figure 12), demonstrating a linear increase of CdS amount with succeeding deposition strokes. This result also implies the high performance of the LB technique in the layer-by-layer control of the particulate deposition through the employment of the present method.

In the literature, trioctylphosphine oxide (TOPO) and alkanelthiols are commonly used as capping agents to manipulate the LB films of semiconductor QDs.[29,50−52] The TOPO-capped CdSe nanoparticles were reported to be able to organize as a hexagonal packed structure due to the higher particle−particle interaction of the chemically modified particles.[50,51] However, morphological heterogeneity or multilayer aggregation is also reported for TOPO-capped CdS[29] and CdSe monolayers,[51] a fact partially ascribed to the lack of amphiphilic property of the QDs. In this work, the 3D aggregates of C_{12}-CdS QDs are more significant than the TOPO-capped CdSe and CdS reported in the literature.[29,51] This phenomenon can be attributed to the interdigitation of dodecyl chains between the surfaces of C_{12}-CdS QDs because 3D aggregates of C_{18}-CdSe were reported to be facilitated through interdigitation of long alkyl chains.[51] Compared to the results of LB manipulation performed through the chemical modification of QDs, the strategy of physical modification presented here offers a more efficient method to assemble nanoparticulate film with characteristics of homogeneity, 2D arrangement, and layer-by-layer control.

Conclusion

CdS QDs were modified either by chemical capping of dodecanethiol (C_{12}-CdS) or by the physical adsorption of CTAB

on MSA-capped CdS (CTAB-MSA-CdS). The two QDs were utilized to investigate the effects of the modification methods on the monolayer behavior and on the performance of LB manipulation. The results show that C_{12}-CdS QDs are not able to spread homogeneously at the air/liquid interface. The 3D aggregative domains and pores were formed due to the poor particle−water interaction. On the other hand, the CTAB-MSA-CdS QDs spread uniformly on the subphase and form a 2D particulate monolayer. The improvement of CTAB-MSA-CdS is attributable to the reversible adsorption of CTAB on MSA-CdS, which renders the QDs with a amphiphilic characteristic at the air/water interface. The CTAB-MSA-CdS QDs also show properties superior to those of C_{12}-CdS in performing a layer-by-layer arrangement of 2D particulate films.

References and Notes

(1) Kamat, P. V. *Chem. Rev.* **1993**, *93*, 267.
(2) Hagfeldt, A.; Gratzel, M. *Chem. Rev.* **1995**, *95*, 49.
(3) Wang, Y.; Herron, N. *J. Phys. Chem.* **1991**, *95*, 525.
(4) Chen, X. Y.; Li, J. R.; Li, X. C.; Jiang, L. *Biochem. Biophys. Res. Commun.* **1998**, *245*, 352.
(5) Hoffman, A. J.; Mills, G.; Yee, H.; Hoffman, M. R. *J. Phys. Chem.* **1992**, *96*, 5546.
(6) Collier, C. P.; Saykally, R. J.; Shiang, J. J.; Henrichs, S. E.; Heath, J. R. *Science* **1997**, *277*, 1978.
(7) Motte, L.; Billouder, F.; Lacaze, E.; Douin, J.; Pileni, M. P. *J. Phys. Chem.* B **1997**, *101*, 138.
(8) Mastai, Y.; Hodes, G. *J. Phys. Chem. B* **1997**, *101*, 2685.
(9) Anderson, M. A.; Gorer, S.; Penner, R. M. *J. Phys. Chem. B* **1997**, *101*, 5895.
(10) Hsiao, G. S.; Anderson, M. G.; Gorner, S.; Harris, D.; Penner, R. M. *J. Am. Chem. Soc.* **1997**, *119*, 1439.
(11) Miyake, H.; Matsumoto, H.; Nishizawa, M.; Sakata, T.; Mori, H.; Kuwabata, S.; Yoneyama, H. *Langmuir* **1997**, *13*, 742.
(12) Nakanishi, T.; Ohtani, B.; Uosaki, K. *J. Phys. Chem. B* **1998**, *102*, 1571.
(13) Hu, K.; Brust, M.; Bard, A. J. *Chem. Mater.* **1998**, *10*, 1160.
(14) Granot, E.; Patolsky, F.; Willner, I. *J. Phys. Chem. B* **2004**, *108*, 5875.
(15) Sheeney-Haj-Ichia, L.; Wasserman, J.; Willner, I. *Adv. Mater.* **2002**, *14*, 1323.
(16) Kumar, N. P.; Narang, S. N.; Major, S.; Vitta, S.; Talwar, S. S.; Dubcek, P.; Amenitsch, H.; Berntorff, S. *Colloids Surf., A* **2002**, *198*−*200*, 59.
(17) Bourgoin, J.-P.; Kergueris, C.; Lefevre, E.; Palacin, S. *Thin Solid Films* **1998**, *327*−*329*, 515.
(18) Reculusa, S.; Ravaine, S. *Chem. Mater.* **2003**, *15*, 598.
(19) Wang, W.; Gu, B.; Liang, L.; Hamilton, W. *J. Phys. Chem. B* **2003**, *107*, 3400.
(20) Stine, K. J.; Moore, B. G. In *Nano-Surface Chemistry*; Rosoff, M., Ed.; Marcel Dekker: New York, 2002; Chapter 3, p 59.
(21) Samokhvalov, A.; Gurney, R. W.; Lahav, M.; Naaman, R. *J. Phys. Chem. B* **2002**, *106*, 9070.
(22) Moriguchi, I.; Nii, H.; Hanai, K.; Nagaoka, H.; Teraoka, Y.; Kagawa, S. *Colloids Surf., A* **1995**, *103*, 173.
(23) Elliot, D. J.; Furlong, D. N.; Grieser, F. *Colloids Surf., A* **1999**, *155*, 101.
(24) Takahashi, M.; Natori, H.; Tajima, K.; Kbayashi, K. *Thin Solid Films* **2005**, *489*, 205.
(25) Tian, Y.; Wu, C.; Fendler, J. H. *J. Phys. Chem.* **1994**, *98*, 4913.
(26) Mayya, K. S.; Sastry, M. *Langmuir* **1998**, *14*, 74.
(27) Tian, Y.; Fendler, J. H. *Chem. Mater.* **1996**, *8*, 969.
(28) Toromoto, T.; Tsumura, N.; Miyake, M.; Nishizawa, M.; Sakata, T.; Mori, H.; Yoneyama, H. *Langmuir* **1999**, *15*, 1853.
(29) Ferreira, P. M. S.; Timmons, A. B.; Neves, M. C.; Dynarowicz, P.; Trindade, T. *Thin Solid Films* **2001**, *389*, 272.
(30) Sbrana, F.; Parodi, M. T.; Ricci, D.; Zitti, E. D. *Mater. Sci. Eng.* **2002**, *C22*, 187.
(31) Grieser, F.; Furlong, D. N.; Scoberg, D.; Ichinose, I.; Kimizuka, N.; Kunitake, T. *J. Chem. Soc., Faraday Trans.* **1992**, *88*, 2207.
(32) Du, Z.; Zhang, Z.; Zhao, W.; Zhu, Z.; Zhang, J.; Jin, Z.; Li, T. *Thin Solid Film* **1992**, *210/211*, 404.
(33) Yamaki, T.; Asai, K.; Ishigure, K. *Chem. Phy. Lett.* **1997**, *273*, 376.
(34) Basu, J. K.; Sanyal, M. K. *Phys. Rev. Lett.* **1997**, *79*, 4617.
(35) Vitta, S.; Metzger, T. H.; Major, S. S.; Dhanabalan, A.; Talwar, S. S. *Langmuir* **1998**, *14*, 1799.
(36) Facci, P.; Fontana, M. P. *Solid State Commun.* **1998**, *108*, 5.
(37) Horozov, T. S.; Aveyard, R.; Clint, J. H.; Inks, B. P. *Langmuir* **2003**, *19*, 2822.
(38) Reculusa, S.; Masse, P.; Ravaine, S. *J. Colloid Interface Sci.* **2004**, *279*, 471.
(39) Tolnai, Gy.; Csempesz, F.; Kabai-Faix, M.; Kalman, E.; Keresztes, Zs.; Kovacs, A. L.; Ramsden, J. J.; Horvolgyi, Z. *Langmuir* **2001**, *17*, 2683.
(40) Szekeres, M.; Kamalin, O.; Schoonheydt, R. A.; Wostyn, K.; Clays, K.; Persoons, A.; Dekany, I. *J. Mater. Chem.* **2002**, *12*, 3268.
(41) Duffel, B. van; Ras, R. H. A.; Schryver, F. C. De; Schoonheydt, R. A. *J. Mater. Chem.* **2001**, *11*, 3333.
(42) Huang, S.; Tsutsui; Sakaue, H.; Shingubara, S.; Takahagi, T. *J. Vac. Sci. Technol. B* **2001**, *19*, 115.
(43) Lee, Y. L.; Du, Z. C.; Lin, W. X.; Yang, Y. M. *J. Colloid Interface Sci.* **2006**, *296*, 233.
(44) Santhanam, V.; Liu, J.; Agarwal, R.; Andres, R. P. *Langmuir* **2003**, *19*, 7881.
(45) Chen, X. Y.; Li, J. R.; Jiang, L. *Nanotechnology* **2000**, *11*, 108.
(46) Huang, S.; Minami, K.; Sakaue, H.; Shingubara, S.; Takahagi, T. *Langmuir* **2004**, *20*, 2274.
(47) Agostiano, A.; Catalano, M.; Curri, M. L.; Monica, M. D.; Manna, L.; Vasanelli, L. *Micron* **2002**, *31*, 253.
(48) Henglein, A. *Chem. Rev.* **1989**, *89*, 1861.
(49) Chen, S.; Kimura, K. *Langmuir* **1999**, *15*, 1075.
(50) Dabbousi, B. O.; Murray, C. B.; Rubner, M. F.; Bawendi, M. G. *Chem. Mater.* **1994**, *6*, 216.
(51) Gattas-Asfura, K. M.; Constantine, C. A.; Lynn, M. J.; Thimann, D. A.; Ji, X.; Leblanc, R. M. *J. Am. Chem. Soc.* **2005**, *127*, 14640.
(52) Ji, X.; Wang, C.; Xu, J.; Zheng, J.; Gattas-Asfura, K. M.; Leblanc, R. M. *Langmuir* **2005**, *21*, 5377.